Gain model for microchannel plates

Edward H. Eberhardt

It is shown that microchannel plates (MCPs) tend to act as if they were discrete stage electron multipliers with a fixed number of stages or dynodes if a plausible assumption is made regarding the behavior of the secondary electrons emitted from the semiconducting sidewalls of tubular channel electron multipliers under the grazing incidence conditions predominantly encountered in these multipliers. The shape of the resultant predicted gain-voltage transfer characteristic for the MCP fits well with experimental data, confirming the assumption made and permitting the use of curve matching techniques to determine such important MCP parameters as the average number of active dynodes, the gain per stage, the crossover potential for the MCP wall material, the transit time through the multiplier, etc.

Introduction

In the cylindrical channel electron multiplier,[1,2] commonly used in the construction of electron image amplifying microchannel plates (MCPs),[3–6] the secondary electrons emitted from one impact area on the side wall of a channel are widely dispersed, both axially and circumferentially, in traveling between channel walls. This spatial dispersion of the electron trajectories is an unavoidable result of the statistical variation of the emission angle and emission energy of the electrons and leads to channel behavior which can only be accurately analyzed by the use of comparatively complicated computerized statistical sampling techniques[7,8] or by the use of complex mathematical approximations[2,9] unless certain simplifying assumptions can be made regarding the emission properties of the secondary electrons.

Analysis

The geometry of one electron trajectory, internal to an MCP channel, is shown in Fig. 1 for the special case in which the trajectory intersects the channel axis. This particular electron travels an axial distance z before striking the opposite wall of the channel, given by

$$z = \frac{ED^2}{4V_{or}}\left[1 \pm \frac{4z}{D}\frac{(V_{or}V_{oz})^{1/2}}{V_z}\right] \tag{1}$$

$$\cong ED^2/4V_{or} \quad \text{for} \quad (V_{or}V_{oz})^{1/2} \ll V_z, \tag{2}$$

where e is the electronic charge, eV_{oz} is the axial emission energy of the electron, eV_{or} is the radial emission energy of the electron, eV_z is the axial energy gain of the electron during transit, D is the channel diameter, and E is the electric field internal to the channel imposed by the flow of strip current in the semiconducting walls of the channel. For the minimal charge flow conditions to be considered here, the electric field E is a constant and is related to V_z and z by

$$E = V_z/z. \tag{3}$$

According to Eq. (2), the axial displacement z is inversely proportional to the radial emission energy eV_{or}, but independent of the axial emission energy eV_{oz}, since eV_{or} and eV_{oz} are, in general, both much smaller than the axial energy gain of the electron eV_z. A similar expression can be derived for the (smaller) axial displacement of an electron traveling a skewed (chord) transit of the channel—this displacement also being inversely proportional to the radial emission energy eV_{or}. The average axial displacement $\bar{z}$ for all electrons making up the emission ensemble from a point on the channel wall can then be expressed in the form

$$\bar{z} = ED^2/4\bar{V}_{or}, \tag{4}$$

where $e\bar{V}_{or}$ is the properly weighted average radial emission energy of the electrons (the weighting process including the smaller distances traveled by skewed electron trajectories). The key property of the channel multiplication process described by Eq. (4) is the reciprocal proportionality between the weighted average energy of the electrons $e\bar{V}_{or}$ and their average axial displacement $\bar{z}$.

Only minimal information is available regarding the magnitude and statistical distribution of the radial emission energy component of secondary electrons emitted under the peculiar near-grazing incidence

The author is with ITT Electro-Optical Products Division, Fort Wayne, Indiana 46803.

Received 13 November 1978.
0003-6935/79/091418-06$00.50/0

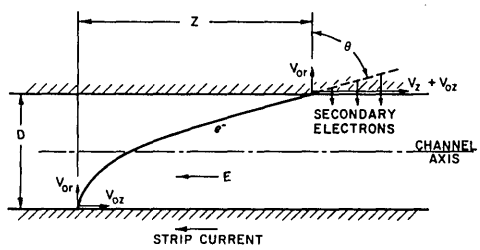

Fig. 1. Typical electron trajectory in a cylindrical channel electron multiplier for an electron trajectory intersecting the channel axis.

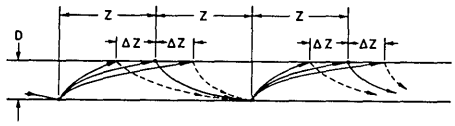

Fig. 2. Focused electron trajectories in a cylindrical channel electron multiplier, predicted on the basis of a direct proportionality between the bombarding primary electron energy and the average radial emission energy of the secondary electrons.

conditions encountered in straight channel electron multipliers. As indicated in Fig. 1, the sole energy component of the bombarding electrons orthogonal to the channel surface (assumed smooth) and, therefore, the sole energy component available for depth penetration of the wall material, is the prior radial emission energy eV_{or}. No energy is added to the electrons by the applied electric field E, which contributes directly to orthogonal penetration of the electrons into the wall. Nearly all other types of electron multipliers, as well as other types of secondary emission devices, depend upon acceleration of the bombarding electrons, by various means, in a direction orthogonal to the bombarded surface, to produce greater depths of penetration. Consequently, the published experimental and theoretical information regarding the secondary emission process is primarily confined to these more deeply penetrating energies and angles.

Pending the availability of appropriate and detailed information on the unusual secondary emission conditions encountered in MCPs, it is nevertheless possible to predict certain key properties of MCPs and to avoid the use of large computers and/or complex statistical sampling techniques by making a plausible assumption regarding the behavior of the secondary electrons encountered in MCPs, namely, that the average radial emission energy $e\bar{V}_{or}$ is proportional to the bombarding electron energy eV_z, according to

$$V_{or} = V_z/4\beta^2, \tag{5}$$

where β is a dimensionless proportionality constant. [In Eq. (5) and in the remaining text the use of the averaging bar notation above a statistically varying parameter has been dropped for notational simplicity.]

The plausibility of this energy proportionality hypothesis follows from the minimal numbers of energy-dissipative interactions which the secondary electrons undergo with the channel wall material in traveling the short distance between their point of origin along the near-surface path of the penetrating primary electron (see Fig. 1) and the surface of the channel. As a result, the emitted secondary electrons can be expected to carry a more significant fraction of the incident electron energy than is usually encountered in the secondary emission process.

With this energy proportionality hypothesis, the average axial displacement z between wall encounters is a constant given by

$$z = \tfrac{1}{2}(V_z/V_{or})^{1/2}D = \beta D \tag{6}$$

and is independent of the applied electric field E and of the applied voltage V between faces of the MCP. With respect to the flow of average electrons, each incremental length z of an MCP channel, therefore, acts as if it were the fixed gap between two discrete bombarded areas, or dynodes. And each over-all MCP section of length L, characterized by an L-over-D ratio, $\alpha(=L/D)$, acts as if it were a discrete stage electron multiplier having a fixed characteristic number of dynodes n, given by

$$n = L/z = (L/D)/(z/D) = \alpha/\beta. \tag{7}$$

This tendency toward a fixed average number of wall encounters, or dynodes, for a given length of channel is strongly reinforced in MCPs by a second property of the channel electron multiplication process also following directly from the energy proportionality hypothesis [Eq. (5)]. An electron whose axial displacement is perturbed from the average displacement z as an unavoidable result of emission energy and emission angle variations, by a small increment Δz (see Fig. 2), will strike the channel wall with a perturbed axial energy, $e(V_z + \Delta V_z)$, given by

$$\Delta V_z/V_z = \Delta z/z. \tag{8}$$

As a result of this altered axial energy the ensemble of secondary electrons triggered by this perturbed electron will have, according to Eq. (5), an altered average radial emission energy, $e(V_{or} + \Delta V_{or})$, given by

$$\Delta V_{or}/V_{or} = \Delta V_z/V_z \tag{9}$$

and a corresponding altered average axial displacement, $z + \Delta z'$, at the next wall-to-wall transit given by

$$\Delta z'/z \cong -\Delta V_{or}/V_{or} \tag{10}$$

such that

$$\Delta z' \cong -\Delta z. \tag{11}$$

Thus any small axial perturbed displacement Δz at one wall-to-wall transit, for any electron, will be followed by a compensating perturbed axial displacement of opposite polarity $-\Delta z$ for the average electron trajectory at the next wall-to-wall transit. The resultant focused, or dynodized, flow of electrons is illustrated in Fig. 2, with the dashed line trajectories for the second wall-to-wall transit designating average trajectories according to the altered average energy, $e(V_{or} + \Delta V_{or})$. This compensating axial perturbation of the electron trajectories also holds for skewed transit of the electrons, although circumferential dispersion, not shown

in Fig. 2, does then occur. Insofar as the energy proportionality hypothesis is correct, the flow of electrons in cylindrical channel multipliers will, therefore, tend to converge or focus toward an average displacement $2z$ after two wall-to-wall transits, i.e., toward an average displacement z for each wall-to-wall transit. Because of the unavoidable axial dispersion which occurs at each emission point on the channel walls, as well as the spatial distribution of electrons over the input to a typical MCP (see below), this dynodizing action will not be discretely detectable along the channel surface. Nevertheless the tendency toward dynodized flow, shown in Fig. 2, will strongly govern the over-all input–output behavior of the MCP, if the energy proportionality hypothesis is correct.

Gain Calculation

As an example of the application of the discrete stage dynodized flow of electrons in MCPs to the analysis of MCP device behavior, consider the expected over-all current gain of a typical MCP used in a proximity focused photomultiplier tube[10] or in a proximity focused image intensifier tube.[11] In the close-space configuration used in these tubes, the channels of the MCP are typically bias cut at an angle ϕ with respect to the face of the MCP (see Fig. 3) such that the bombarding photoelectrons incident on the face of the MCP penetrate the MCP holes to a maximum depth of $D\cot\phi$ and trigger a flow of secondary electrons characterized by a maximum of $(L/z) + 1$ and a minimum of $(L - D\cot\phi)/z$ dynodes. For the special and experimentally realistic case in which the bias cut angle ϕ is selected to match the complement of the incident angle θ (typically 5–10°), for the average secondary electrons given by

$$\tan\theta = (V_z/V_{or})^{1/2} = 2\beta, \tag{12}$$

the hole-axis-entering electrons penetrate each channel to a depth equal to one dynode spacing distance z and strike the channel wall at the same incident angle as the subsequent average secondary electrons (see Fig. 3). The average total number of dynodes contributing to the gain process is then approximately equal to the characteristic number of dynodes n given by Eq. (7) for a channel of length L. . More deeply penetrating electrons will undergo fewer wall encounters, and less deeply penetrating electrons will undergo more encounters, but, on the average, a bias-cut MCP under these conditions can be expected to act almost as if it were a discrete stage electron multiplier with $n(=L/z = \alpha/\beta)$ dynodes.

By analogy with the known behavior of discrete staged electron multipliers, the gain G of an MCP can then be approximated by the power law relationship

$$G = \delta_1\delta^{n-1}, \tag{13}$$

where δ_1 is the effective gain per stage for the input photoelectrons (including gains or losses of photoelectrons striking the input web areas of the MCP), and δ is the effective gain per stage for the internal cascaded electron multiplication processes, exclusive of the first stage.

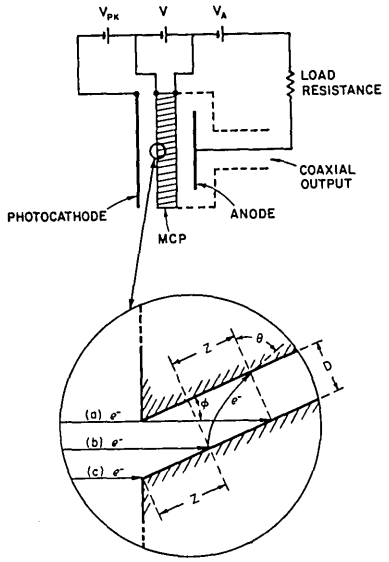

Fig. 3. Operating configuration of an MCP photomultiplier tube with the insert showing the photoelectron incidence conditions on one channel of the MCP.

This relationship can be converted to the gain-voltage transfer characteristic of the MCP if sufficient data are available regarding the shape of the secondary emission function $\delta(V_z)$. While the magnitude of this function varies considerably for various secondary emission materials, the general shape for low bombarding energies can usually be approximated by

$$\delta = (V_z/V_c)^k \tag{14}$$

with an analogous function

$$\delta_1 = \gamma[(V_{pk} + V_z)/V_c]^k \tag{15}$$

for the input photoelectrons, where V_c is the so-called first crossover potential (i.e., the minimum potential for unity secondary emission ratio), eV_{pk} is the input energy of the photoelectrons, γ is the effective electron acceptance area ratio for the MCP, and k is a constant coefficient given by the curvature of the secondary emission function $\delta(V_z)$ over the range of operating potential differences encountered.

The preceding relationships lead to the following general expression for the gain-voltage transfer characteristic of an MCP:

$$G = \delta_1(V/nV_c)^{k(n-1)} = \gamma[(nV_{pk} + V)/nV_c]^k(V/nV_c)^{k(n-1)}. \tag{16}$$

Perhaps the most striking property of the MCP, predicted by Eq. (16), with k, n, γ, V_{pk}, and V_c being constants, is the continued increase in the gain G with applied voltage V, with no tendency to maximize. Channel saturation effects, which invariably occur due to wall charge depletion and/or space charge buildup at high gains and/or high current levels, and which eventually invalidate the constant E-field assumption, Eq. (3), are not considered here. Prior mathematical approximations (Refs. 3–5, 9, and 12–14) for the gain-voltage transfer characteristic, derived under the same

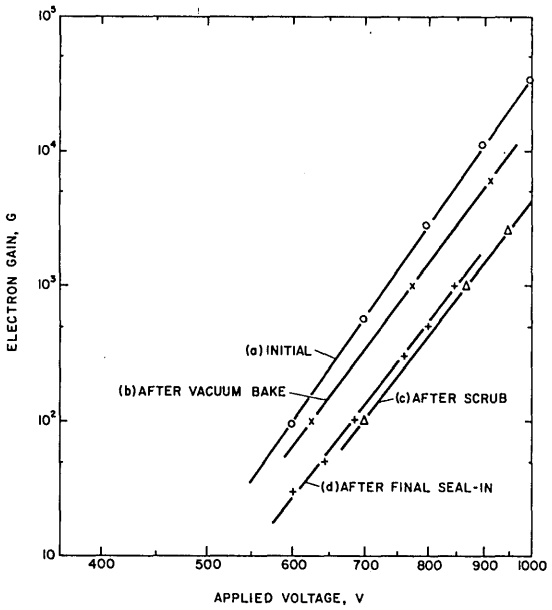

Fig. 4. Measured gain vs applied voltage for an MCP (ITT MCP 671) after several steps in the manufacturing procedure. The straight line plots are computed from the MCP parameters listed in Table I, with $\alpha = 40$ and $k = 0.75$.

constant E-field assumption, have either indicated instead that the gain should maximize at a finite operating voltage, and subsequently decrease, a behavior not consistent with Eq. (16) and not reported in the literature, or they are not explicit regarding the expected change in gain with voltage. The steadily increasing gain-voltage behavior predicted from Eq. (16) does fit qualitatively with the experimental behavior and the computer-based estimates of MCP performance reported by Guest[7] and with the general experimental behavior reported by other authors.[3,4,6,12–14]

For most practical applications of MCPs, the input voltage V_{pk} for the photoelectrons is selected to be comparatively large, i.e., greater than 150–200 V, compared with the voltage per stage V_z typically encountered (e.g., 40–50 V, see below). The general relationship, Eq. (16), between G and V can then be approximated by a linear proportionality between $\log G$ and $\log V$:

$$\log G \cong k(n-1)\log(V/nV_c) + \log\gamma(V_{pk}/V_c)^k. \quad (17)$$

According to this approximation if $\log G$ is plotted vs $\log V$, instead of the usual plot of $\log G$ vs V, the data will conform to a straight line with a slope equal to $k(n-1)$ and with an intercept voltage equal to nV_c on the $G = \gamma(V_{pk}/V_c)^k \cong \delta_1$ axis. Slope and intercept measurements can then be used on best fit straight data line plots to determine conveniently $k(n-1)$ and nV_c for a particular MCP. And if an independent estimate is available regarding the numerical magnitude of the secondary emission curvature constant k, these slope and intercept measurements also determine the number of dynode stages n, the first crossover potential V_c, as well as other characteristic MCP parameters, such as the relative dynode spacing ratio β, the incident angle θ, and the time of flight t between wall encounters given by

$$t = D(2m\alpha\beta)^{1/2}/(\mathrm{eV})^{1/2}, \quad (18)$$

where m is the electron mass. The numerical magnitude of the first crossover potential V_c is particularly significant in evaluating the relative performance of MCP wall materials, as secondary emitters, compared with more conventional dynode materials such as AgMgO and CuBeO etc.

Experimental

The input–output current gain of an ITT-manufactured 18-mm diam MCP (671) was observed as a function of the applied voltage following four steps in the manufacturing process, leading to the completion of a sealed-off MCP photomultiplier tube (type F-4126). The input current to the MCP, at 150-V accelerating potential and with orthogonal electron incidence, was measured directly with a sensitive ammeter, and the output current was measured with sufficient collecting voltage (above approximately 100 V) to assure saturated collection of all emitted secondary electrons and at average output current levels low enough (i.e., below approximately $10nA$) to assure maintenance of the constant E-field within each channel. The observed data, appearing as the plotted points in Fig. 4, show a pronounced tendency toward linear $\log G$ vs $\log V$ behavior, as predicted by the energy proportionality hypothesis.

The measured slope $k(n-1)$ and the measured voltage intercept nV_c for the four best-fit straight line plots in Fig. 4 are listed in Table I along with the derived magnitudes of the MCP-characterizing parameters n, V_c, β, and θ. In computing these derived parameters, a secondary emission curvature coefficient k equal to 0.75 was, somewhat arbitrarily, assumed based on (unreported) experimental measurements made in our laboratory on more conventional secondary emitters such as AgMgO and CuBeO, but not on typical MCP wall materials. Guest[7] has assumed a somewhat larger coefficient, i.e., $k = 1.0$, for MCP wall materials, and Schagen[4] has assumed a somewhat lower coefficient, i.e., $k = 0.5$, but without supporting experimental evidence. A more accurate determination of the derived parameters will require correspondingly more accurate data regarding the magnitude of the curvature coefficient k. The intercept voltage, at nV_c on the $G = \delta_1$ axis for the four straight line plots in Fig. 4 and thus the magnitude of the first crossover potential V_c, was determined by a series of successive approximations, first assuming an initial value for the secondary emission ratio δ_1 (e.g., 3.0) for the input photoelectrons, then finding the corresponding intercept voltage nV_c (and thus V_c), and then calculating a corrected value of δ_1 from Eq. (14). An effective electron acceptance area ratio γ equal to the geometric open area ratio (0.6) for this MCP was assumed in Eq. (14), ignoring the probable contribution

Table I. Gain Parameters of an MCP During Manufacture

Process step	*a* Initial	*b* After vacuum bake	*c* After electron scrub	*d* Final tube	Units
Gain-voltage slope $k(n-1)$	11.5	11.1	10.3	11.4	—
Voltage intercept nV_c	435	442	473	476	Volts
Number of dynodes n	16.3	15.8	14.7	16.2	—
Crossover potential V_c	26.7	28.0	32.2	29.4	Volts
Spacing ratio β	2.45	2.53	2.72	2.47	—
Incident angle θ	78.5	78.8	79.6	78.6	Degrees
Input gain δ_1	2.19	2.11	1.90	2.04	—

Table II. Operating Parameters of an MCP in a Sealed-off Photomultiplier Tube

				Units
Gain G	100	300	1000	—
Applied voltage V	671	738	821	Volts
Voltage/stage V_z	41.4	45.6	50.7	Volts
Gain/stage δ	1.29	1.39	1.51	—
Transit time nt	0.25	0.24	0.23	nsec
Emission energy eV_{or}	1.70	1.87	2.08	eV
Peak output current I_m	8.6	9.9	11.5	A

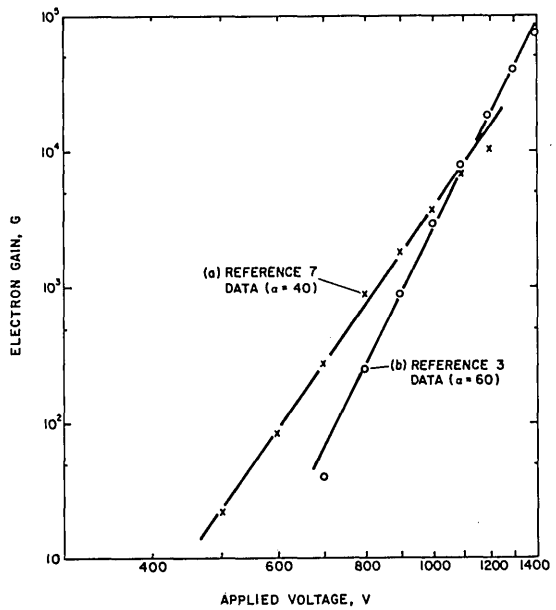

Fig. 5. Comparison between calculated MCP gain vs voltage (straight lines) and previously reported experimental MCP data (plotted points). The MCP parameters used for computing the gain are listed in Table III.

to the MCP gain of the secondary electrons emitted from the web areas of the MCP reported by Panitz and Foesch.[15] The final magnitude of the first crossover potential V_c obtained in this manner is not particularly sensitive to the assumed magnitude of γ. A correction for partial penetration of the input and output conductive electrodes into the MCP holes (i.e., an end-spoiling correction) was made in computing the effective L/D ratio, α (=40), for this MCP.

Examination of the results tabulated in Table I shows that the MCP tested acted almost as if it were a conventional 16-stage electron multiplier (i.e., similar to the electron multiplier in an ITT FW130 photomultiplier tube) at all steps in the MCP processing, corresponding to a relative dynode spacing ratio α of 2.5 channel diameters. Perhaps the most significant change in this MCP during the manufacturing process was the increase, i.e., degradation, in the first crossover potential V_c from 26.7 V initially to 29.4 V after final tube assembly. Although both magnitudes are characteristic of moderately high gain secondary emissive materials, the observed increase in V_c was sufficient to cause a loss of almost an order of magnitude in the over-all gain G at a fixed voltage V during processing.

Operating MCP parameters, such as the gain per stage δ and the voltage per stage V_z, which depend upon the selected MCP operating conditions, are listed in Table II for three representative gains: 100, 300, and 1000. The computed gains per stage of 1.29 to 1.51 are somewhat small compared to operating conditions usually selected for more conventional types of electron multipliers, but are sufficient to maintain the SNR established primarily by the first encounter of the photoelectrons with the MCP. Also listed in Table II is the computed total input–output transit time nt (approximately 0.25 nsec) for the average electron flow in the MCP from Eq. (18) (with $D = 1.25 \times 10^{-5}$ m).

A rough estimate of the peak output charge per channel Q_m, available from the MCP, can be made by assuming that the available charge for a fast pulse input is stored on a parallel plate capacitor with a spacing equal to β channel diameters operating at V_z potential difference. For the plate evaluated this charge equals approximately 10^4 electrons per channel or 10^{-9} C for the 18-mm diam area (with approximately 1.5×10^6 channels). If this charge is delivered to the output from the MCP in the total transit time nt, the peak output current listed in Table II (approximately 10 A) is obtained. Peak currents within an order of magnitude of this predicted maximum have been observed on this type of photomultiplier tube, subject to the limitations on the maximum average output current established by the strip current limits (approximately 1–2 μA/cm^2).

As a further check of the validity of the energy proportionality hypothesis, the experimental MCP gain vs voltage data reported by Guest[7] on $\alpha = 40$ MCPs and by Eschard and Manley[3] on $\alpha = 60$ MCPs (below 1400 V) is replotted in Fig. 5, using a log$G$ vs log$V$ technique instead of the log$G$ vs V technique selected by these authors. While some departure from linearity is apparent, especially at the higher gain levels where

Table III. Comparative MCP Gain Parameters

Author	Present work (final) tube)	Guest[7]	Eschard and Manley[3]	Units
Input voltage V_{pk}	150	2000	5000	Volts
L/D ratio α	40	40	60	—
Gain-voltage slope $k(n-1)$	11.4	7.20	10.8	—
Number of dynodes n	16.2	10.61	15.4	—
Dynode spacing ratio β	2.47	3.77	3.89	—
Crossover potential V_c	29.4	46.1	44.6	Volts
Incident angle θ	78.6	82.5	82.7	Degrees
Input gain δ_1	2.04	10.1	20.7	—

channel saturation may be beginning, the basic behavior again appears to be linear. The derived MCP-characterizing constants, n, V_c, β, and θ for the best fit straight line plots in Fig. 5 are listed in Table III, the dynode spacing ratio β being essentially constant (at 3.8), and the first crossover potential V_c also being approximately constant (at 45 V). Thus it appears that the MCP wall material was nominally identical for these two types of MCPs despite the sharp differences in gain and in gain slope exhibited in Fig. 5. It also appears that the MCP wall material was significantly different than the wall material used for the ITT MCP, both β and V_c being significantly larger in magnitude.

Summary

The assumption that the average radial emission energy of the secondary electrons emitted from the sidewalls of channel electron multipliers is proportional to the incident bombarding energy leads to predicted microchannel plate (MCP) behavior, which fits well with initial experimental data. Perhaps the most interesting and useful property of the predicted MCP gain process, not previously reported in the technical literature, is the tendency of the secondary electrons to focus or converge toward band areas or dynodes along the channel walls, located at fixed axial increments, such that the MCP tends to act as if it were a conventional discrete stage electron multiplier. If this tendency toward dynodized behavior in MCPs is confirmed by further experimental data, it becomes possible to determine reliably many important properties of the MCP electron multiplication process, such as the average gain per stage, the magnitude of the first crossover potential for the MCP secondary emitting wall material, the total transit time through the multiplier, etc.

References

1. P. T. Farnsworth, U.S. Patent 1,969,399, Filed 30 March 1930.
2. J. M. Grant, in *Proceedings of NASA ERDL Image Intensifier Symposium, 24–26 October 1961* (NASA Office of Scientific and Technical Information, Wash., D.C.), p. 63.
3. G. Eschard and B. W. Manley, Acta Electron. **14,** 19 (1971).
4. P. Schagen in *Advances in Image Pickup and Display, Vol. 1,* B. Kazan, Ed. (Academic, New York, 1974), p. 1–69.
5. W. E. Baumgartner and W. K. Huber, J. Phys. E **9,** 321 (1976).
6. B. Leskovar, Phys. Today **30,** No. 11, 42 (1977).
7. A. J. Guest, Acta Electron. **14,** 79 (1971).
8. W. M. Sackinger, Doctoral Thesis, Cornell U. (1969).
9. J. Linder, Doctoral Thesis, L'Ecole Polytechnique Federale, Zurich (1965) (Prom. No. 3648).
10. J. P. Boutot and G. Pietri, IEEE Trans. Electron Devices **ED-17,** 493 (1970).
11. G. Eschard and J. Graf, *Adv. Electron. Electron Phys.* **28A,** 499 (1969).
12. J. Adams and B. W. Manley, IEEE Trans. Nucl. Sci. **13,** 88 (1966).
13. P. B. Soul, Nucl. Instrum. Methods **97,** 555 (1971).
14. D. J. Ruggieri, IEEE Trans. Nucl. Sci. **19,** 74 (1972).
15. J. A. Panitz and J. A. Foesch, Rev. Sci. Instrum. **47,** 44 (1976).

James G. Davidson
Macbeth (Color Communications) Division
Kollmorgen Corporation